HHS Public Access

Author manuscript

Cell Rep. Author manuscript; available in PMC 2025 May 14.

Published in final edited form as:

Cell Rep. 2021 June 15; 35(11): 109238. doi:10.1016/j.celrep.2021.109238.

NADK is activated by oncogenic signaling to sustain pancreatic ductal adenocarcinoma

Tanya Schild[1,2,3], **Melanie R. McReynolds**[4], **Christie Shea**[1,2,5], **Vivien Low**[1,2,3], **Bethany E. Schaffer**[1,2], **John M. Asara**[6], **Elena Piskounova**[1,3,7], **Noah Dephoure**[3], **Joshua D. Rabinowitz**[4], **Ana P. Gomes**[8,*], **John Blenis**[1,2,9,*]

[1]Meyer Cancer Center, Weill Cornell Medicine, New York, NY 10021, USA

[2]Department of Pharmacology, Weill Cornell Medicine, New York, NY 10021, USA

[3]Department of Biochemistry, Weill Cornell Medicine, New York, NY 10021, USA

[4]Department of Chemistry, Princeton University, Princeton, NJ 08540, USA

[5]Tri-institutional PhD Program in Chemical Biology, New York, NY 10021, USA

[6]Department of Medicine, Beth Israel Deaconess Medical Center and Harvard Medical School, Boston, MA 02215, USA

[7]Department of Dermatology, Weill Cornell Medicine, New York, NY 10021, USA

[8]Department of Molecular Oncology, H. Lee Moffitt Cancer Center & Research Institute, Tampa, FL 33612, USA

[9]Lead contact

SUMMARY

Metabolic adaptations and the signaling events that control them promote the survival of pancreatic ductal adenocarcinoma (PDAC) at the fibrotic tumor site, overcoming stresses associated with nutrient and oxygen deprivation. Recently, rewiring of NADPH production has been shown to play a key role in this process. NADPH is recycled through reduction of NADP+ by several enzymatic systems in cells. However, *de novo* NADP+ is synthesized only through one known enzymatic reaction, catalyzed by NAD+ kinase (NADK). In this study, we show that oncogenic KRAS promotes protein kinase C (PKC)-mediated NADK phosphorylation, leading to

*Correspondence: ana.gomes@moffitt.org (A.P.G.), job2064@med.cornell.edu (J.B.).

AUTHOR CONTRIBUTIONS

T.S., A.P.G., and J.B. conceived the project and designed the experiments. T.S. performed most of the experiments. M.R.M. processed, ran, and analyzed the tracing experiments. C.S. adapted the NADK activity assay. V.L. prepared the samples, J.M.A. performed the mass spectrometry, and A.P.G. analyzed the metabolomic experiments. N.D. performed the mass spec analysis of NADK phosphorylation. T.S., M.R.M., B.E.S., and A.P.G. analyzed the data. A.P.G., N.D., J.D.R., E.P., and J.B. supervised the project. The manuscript was written by T.S. and A.P.G. and edited by V.L., B.E.S., and J.B. All authors discussed the results and approved the manuscript.

SUPPLEMENTAL INFORMATION

Supplemental information can be found online at https://doi.org/10.1016/j.celrep.2021.109238.

DECLARATION OF INTERESTS

J.D.R. is a founder of Raze Therapeutics and advisor to L.E.A.F. Pharmaceuticals, Pfizer, Agios Pharmaceuticals, Kadmon Pharmaceuticals, and Rafael Pharmaceuticals. No potential conflicts of interest were disclosed by the other authors.

its hyperactivation, thus sustaining both NADP+ and NADPH levels in PDAC cells. Together, our data show that increased NADK activity is an important adaptation driven by oncogenic signaling. Our findings indicate that NADK could serve as a much-needed therapeutic target for PDAC.

In brief

Schild et al. show that increased NADP+ synthesis is an adaptation powering PDAC. NADP+ synthesis is mediated by NAD+ kinase (NADK) downstream of mutant KRAS. NADK becomes phosphorylated by PKC downstream of oncogenic KRAS to drive anabolic and antioxidant potentials.

Graphical abstract

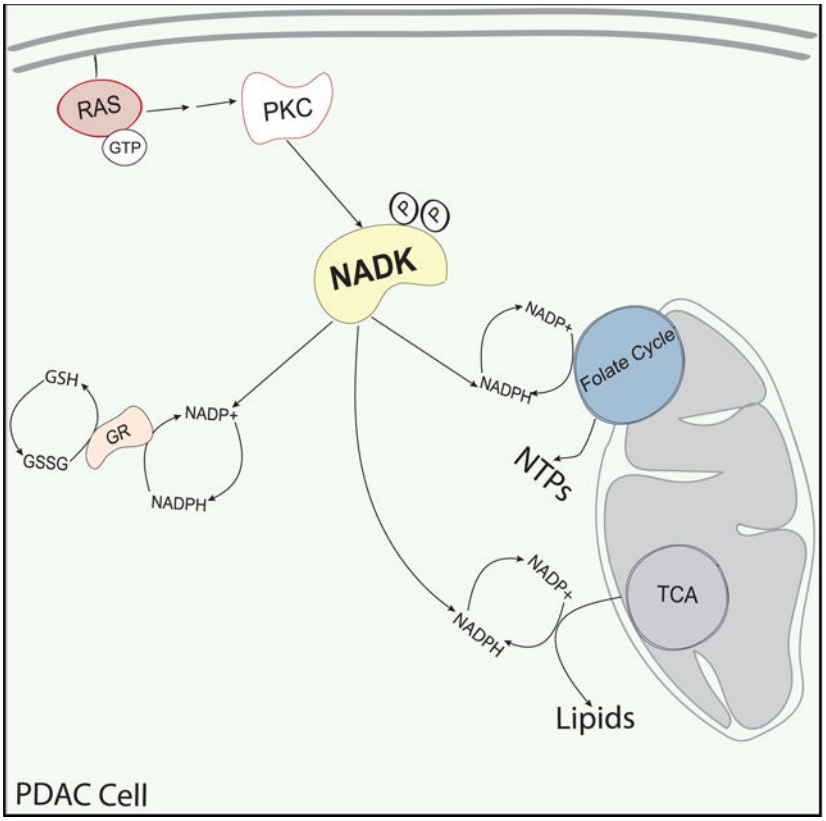

INTRODUCTION

All cancer cells face unique metabolic requirements that vary across different stages of tumorigenesis. However, difficult-to-treat tumors, such as pancreatic ductal adenocarcinomas (PDACs), are notorious for their ability to adapt metabolic flux to counteract nutrient deprivation, oxidative stress, and chemotherapy treatments. RAS, the main oncogenic driver of PDAC, is especially known for its ability to shift the metabolic flux of tumors to support the tumorigenic and metastatic potentials (DeNicola et al., 2011; Ying et al., 2012; Son et al., 2013; Commisso et al., 2013; Palm et al., 2015; Santana-Codina et al., 2018).

NADPH is a metabolic co-factor of particular interest, as it is essential for powering the biosynthesis of macromolecules as well as for maintaining redox homeostasis. Proliferation and cell survival are dependent on the continued generation of NADPH (Ying, 2008). Thus, cells have several well-characterized enzymatic reactions that generate NADPH through reduction of NADP+, providing a constant supply of NADPH (Ying, 2008). However, in rapidly dividing cells, such as cancer cells, recycling of NADP+/NADPH through these systems is unlikely to be sufficient for the levels of NADPH necessary for high rates of biosynthesis and elevated redox requirements. NADPH is not known to be *de novo* produced in humans—however, NADP+ can be *de novo* synthesized in cells through a single known mechanism. NAD+ kinase (NADK) catalyzes the production of NADP+ through the addition of a phosphate moiety from a nucleotide donor, typically ATP, onto the 2′ position of NAD+ (Lerner et al., 2001; Pollak et al., 2007; Love et al., 2015). This reveals a potential role for NADK as a critical regulator of tumorigenesis, particularly in cancers driven by powerful inducers of proliferation, such as oncogenic RAS. Supporting this idea, two recent studies have shown that depleting NADK in PDAC and colon cancer, which are cancers typically driven by oncogenic RAS, results in growth hindrance and in a decreased tumorigenic potential (Tsang et al., 2016; Yau et al., 2017). Despite these observations, NADK's complete role in cellular homeostasis and its contribution to the metabolic rewiring that occurs during tumorigenesis remain largely unknown. Regulation of NADK by oncogenic signaling also remains chiefly unexplored.

RESULTS

Oncogenic KRAS promotes *de novo* NADP+ synthesis

Several studies have suggested that preserving NADPH levels is an important metabolic adaptation of PDAC (DeNicola et al., 2011, 2015; Son et al., 2013). Considering the importance of NADPH for biosynthesis and redox control, both of which support tumorigenesis, we hypothesized that maintaining levels of NADP+ is also important for PDAC pathophysiology. We therefore sought to understand if PDAC requires *de novo* NADP+ synthesis to sustain NADPH levels. To test this, we measured NADP+ and NADPH levels in $KRAS^{G12V}$-transformed pancreatic ductal epithelial cells (PDEs) and in mouse embryonic fibroblasts (MEFs) expressing the oncogenic $KRAS^{G12D}$ mutation. In both cases, induction of oncogenic KRAS led to an increase in the total pools of NADP+ and NADPH (Figures 1A and S1A). Conversely, KRAS knockdown in PANC-1 resulted in a decrease in total NADP+ and NADPH pools (Figure 1B), suggesting that more than simply relying on NADP+/NADPH cytosolic interconversion, PDAC promotes its *de novo* synthesis. Although NADPH is not known to be produced *de novo* from NADH in the cytosol, cytosolic NADP+ is known to be produced by phosphorylation of NAD+. To further explore the connection between oncogenic KRAS and *de novo* NADP+ synthesis, we traced the incorporation of label from deuterated nicotinamide, [^{2}H]NAM, into the NADP+ and NADPH pools (Liu et al., 2018; Figure 1C). Upon transformation with $KRAS^{G12V}$, PDEs had increased label incorporation into NADP+ and NADPH (Figure 1D; Table S1), demonstrating that *de novo* NADP+ synthesis is regulated by KRAS and implicating this process in PDAC pathogenesis.

NADK mediates KRAS-induced *de novo* NADP+ synthesis

De novo NADP+ synthesis is catalyzed by two mammalian NADK isoforms, namely, the cytosolic NADK and the mitochondrial NADK2, leading us to hypothesize that oncogenic KRAS may regulate one or both NADK enzymes to promote *de novo* NADP+ synthesis. Genetic screens aimed at finding effectors of mutant KRAS-driven tumorigenesis identified NADK as a hit (Tsang et al., 2016; Yau et al., 2017) suggesting that NADK, and not NADK2, is the enzyme responsible for the observed increase in *de novo* NADP+ formation driven by oncogenic KRAS. To test if this is indeed the case, we knocked down NADK in PDAC cell lines. We found that knockdown of NADK resulted in a reduction of NADP+ pools in PANC-1 and MIA PaCa-2 cells, whereas overexpression of NADK rescued this effect (Figures 1E and S1E). Moreover, knockdown of NADK in PDAC cells resulted in diminished colony-forming capacity in 3D, in decreased organoid number, and in reduced tumor volume *in vivo* (Figures 1F and 1G). Consistent with the idea that NADK mediates the *de novo* NADP+ synthesis induced by oncogenic KRAS, NADK overexpression was sufficient to rescue the decrease in the total pools of NADP+ and NADPH elicited by knockdown of KRAS in PDAC cells (Figure 1H). Further supporting NADK as the main driver of *de novo* NADP+ production driven by oncogenic KRAS in PDAC, knockdown of NADK2 affected PDAC growth to a lesser degree (Figure S1H). Together, these data show that KRAS relies on NADK to increase the pools of NADP+ that are necessary to maintain the supply of NADPH.

NADK is regulated by KRAS through PKC-mediated phosphorylation

Having demonstrated that NADK is important for KRAS-induced *de novo* NADP+ synthesis, we sought to determine if and how KRAS regulates NADK activity. Considering that NADK was recently shown to be phosphorylated and thereby activated by insulin signaling (Hoxhaj et al., 2019), we postulated that oncogenic RAS may regulate NADK in a similar fashion. To test this, we monitored NADK phosphorylation in PDAC cells after mutant KRAS expression using liquid chromatography-tandem mass spectrometry (LC-MS/MS). We observed an increase in NADK phosphorylation on several residues upon expression of KRAS (Figure 2A; Table S2), further supporting the idea that oncogenic KRAS regulates NADK through phosphorylation. The N-terminal region of NADK, suggested to be the regulatory region (Love et al., 2015; Hoxhaj et al., 2019), contains five putative AGC family kinase sites (Figure 2B). As RAS acts upstream of many AGC family kinases, we hypothesized that one or more AGC kinases may mediate the phosphorylation of NADK downstream of oncogenic RAS induction. To test this, we stimulated serum-starved PDEs with insulin, phorbol 12-myristate 13-acetate (PMA), and serum, of which all are known activators of various AGC kinases. We observed that out of the three stimulants, PMA produced the most robust phosphorylation of NADK (Figure 2C). Insulin, which was previously shown to regulate NADK phosphorylation in breast and lung cancer cells (Hoxhaj et al., 2019), had little observable effect in PDAC cells, suggesting different cancer cells use highly tailored, cell-type-specific mechanisms to regulate NADK, highlighting the importance of this enzyme (Figure 2C). Because PMA directly activates the AGC kinase protein kinase C (PKC), we next investigated whether PKC is responsible for NADK phosphorylation. To this end, we immunoprecipitated NADK and probed its phosphorylation status by using a PKC substrate antibody, which

recognizes the PKC consensus phosphorylation motif R/KXpSXR/K (Figure S2A). PMA and $KRAS^{G12V}$ expression increased the antibody signal, whereas the pan-PKC inhibitor Sotrastaurin abrogated it, suggesting that KRAS-induced NADK phosphorylation is likely dependent on PKC (Figure 2D). This also correlated with PKC activation under the same conditions (Figure S2B). Other PKC activators, such as hydrogen peroxide and ionomycin, resulted in phosphorylation of NADK (Figure S2C), and no other inhibitor tested, besides the PKC inhibitor, decreased the phosphorylation to the baseline level (Figure S2D). In line with the hypothesis that PKC directly phosphorylates NADK, *in vitro* kinase assays showed that PKC robustly phosphorylates NADK (Figure S2E). Conversely, PKC inhibition in PDAC cells also resulted in decreased NADK phosphorylation (Figure 2E). PKC activation by PMA increased label incorporation from [^{2}H]NAM into NADP+ and NADPH, signifying *de novo* NADP+ synthesis in PDAC cells, an effect that was completely blunted by PKC inhibition (Figure 2F). Similarly, KRAS knockdown in PANC-1 cells led to decreased *de novo* NADP+ synthesis that was rescued by PMA addition, supporting the relevance of the KRAS-PKC-NADK regulatory circuit to sustain the heightened need for NADP(H) of PDAC cells (Figure 2G).

PKCs γ and δ phosphorylate NADK in PDAC

We next wanted to determine which PKC isoform phosphorylates NADK. Because calcium signaling, through treatment with a calcium ionophore, ionomycin, resulted in NADK phosphorylation (Figure S2C), we hypothesized that conventional PKC isoforms are the main drivers of NADK phosphorylation in PDAC. Expression analysis of the conventional PKC isoforms α, β, and γ in PDAC cell lines demonstrated that PKC α and γ are expressed, whereas PKC β is not readily detected (Figure 2H). Knockdown of each conventional PKC isoform demonstrated that only PKC γ silencing impacted NADK phosphorylation (Figure 2I). Although novel PKC isoforms are not activated by calcium, they are activated by PMA, so we sought to determine if they are involved in NADK phosphorylation. In the pancreatic compartment, only PKC δ was robustly activated by PMA, as detected by its translocation to the membrane compartment after PMA treatment (Figure S2F). Its silencing lead to a similar decrease in NADK phosphorylation, as was observed upon suppression of PKC γ (Figure 2I), leading to the conclusion that in PDAC both PKC γ and PKC δ mediate NADK phosphorylation.

NADK activity is regulated by S46/S64 phosphorylation

To determine the sites of PKC-mediated NADK phosphorylation, we performed another LC-MS/MS analysis on NADK following PMA stimulation. Similarly to oncogenic KRAS expression, PMA treatment resulted in phosphorylation of serine 46 and serine 64 (Figures 3A and S3A). We further validated this finding through systematic mutation of every AGC kinase site on the N terminus of NADK. Through Phos-tag immunoblot and immunoblot with the PKC substrate antibody, we observed that mutation of serine 46 and serine 64 resulted in a blunted PMA-induced phosphorylation of NADK, as compared to other serines (Figure 3B). In addition, in S46A and S64A NADK mutants, PKC-induced NADK phosphorylation was severely abrogated in *in vitro* kinase assays (Figures 3C and S3B). To test if phosphorylation of NADK at S46 and S64 is an important mediator of PDAC tumorigenesis, we evaluated if expression of the S46A/S64A NADK phosphomutant affects

PDAC tumor burden *in vivo*. When compared to wild-type (WT) NADK, overexpression of the S46A/S64A mutant resulted in reduced tumor volume (Figure 3D). We next wanted to uncover how these events regulate NADK. To test this, we analyzed the NADK phosphomutants functionally. When both S46 and S64 were mutated to alanines, PMA-induced increase in total NADP+ and NADPH pools, as well *de novo* NADP+ synthesis, were completely abrogated (Figures 3E and 3F). It is important to note that neither S46A and S64A single mutants nor a double mutant containing a different serine (S48A/S64A) were able to block the PMA-induced increase in NADP+ and NADPH pools, demonstrating that S46 and S64 phosphorylation cooperate to regulate NADK in response to PKC activation (Figures 3E and 3G). Interestingly, only the phosphomimetic S64D, but not S46D mutation, resulted in elevated NADP+ and NADPH levels (Figure S3C), indicating that phosphorylation at S46 is likely priming for phosphorylation of the main regulatory NADK residue S64. Surprisingly, expression of the S46D/S64D NADK mutant also resulted in reduced tumor volume when compared to WT NADK (Figure S3D), possibly signifying that *in vivo* the mutant is not recapitulating the physiology of the phosphorylation. Another possibility is that too much NADK activity is deleterious *in vivo*. To determine if these phosphorylation events regulate *de novo* NADP+ synthesis directly by regulating NADK enzymatic activity, we performed *in vitro* measurements of NADK activity by using NADK WT, S46A, or S64A protein purified from PMA-stimulated cells (Figure S3E; Lerner et al., 2001; Pollak et al., 2007; Love et al., 2015). Although the Michaelis constants were not significantly different—1.5 for WT, 1.3 for S46A, and 1.5 for S64A—the maximum velocity (V_{max}) achieved by each mutant was lower than that of WT NADK (Figure 3H). These observations suggest that phosphorylation of S46 and S64 work by changing the rate of NAD+ conversion to NADP+ rather than by altering the affinity of NADK for NAD+. Altogether, these data indicate that phosphorylation of S46 and S64 on NADK regulates its enzymatic activity to induce *de novo* NADP+ production, enabling PDAC tumorigenesis.

NADK contributes to antioxidant and biosynthetic processes in PDAC

Considering the importance of NADK regulation in PDAC, we set out to identify the metabolic processes that rely on NADK in oncogenic KRAS-driven PDAC cells. We suppressed NADK in PDAC cells and performed targeted metabolomics. This analysis revealed a significant metabolic remodeling upon NADK knockdown (Figure 4A). Pathway enrichment analysis showed that NADK powers several biosynthetic processes such as nucleotide and lipid biosynthesis, as well as resistance to oxidative stress (Figure 4B; Table S3). Measurements of glutathione showed a pronounced decrease following NADK knockdown in oncogenic KRAS-driven PDAC cells, whereas no effect was observed in KRAS WT PDAC cells (Figures 4D and S4B). Similarly, lipid and nucleotide profiling showed a pronounced decrease in several nucleotides and lipid species in MIA PaCa-2 (a $KRAS^{G12C}$ PDAC cell line), whereas either a minimal effect or the opposite effect was observed in BxPC3 (a $KRAS^{WT}$ PDAC cell line), implying a specific importance of NADK in oncogenic KRAS-driven PDAC cells (Figures 4E, 4G, 4H, S4C, and S4D; Tables S3 and S4). Having determined which metabolic pathways sustained by NADK activity are important in oncogenic KRAS-driven PDAC cells, we sought to determine if deregulation of these processes is at the root of the decline in tumor growth upon NADK suppression. Supplementation with nucleosides, lipids, or a powerful antioxidant (N-acetylcysteine) alone

was not sufficient to rescue the defect in 3D colony formation elicited by knockdown of NADK, indicating that NADK's effects are multifactorial (Figure 4I). In line with this finding, supplementation with a combination of nucleosides, lipids, and N-acetylcysteine partially rescued the colony growth of PDAC cells lacking NADK (Figure 4I). Finally, we sought to understand the broader relevance of NADK across tumor types and found that in addition to PDAC, NADK promotes the growth of melanoma and lung adenocarcinomas, driven by multiple oncogenes including the RAS, RAF, and EGFR (Figure S4G). Together, our work demonstrates that NADK supports NADP(H) metabolism in PDAC, with likely roles in additional cancer types and suggests that NADK can serve as a specific and effective therapeutic target in KRAS-driven PDAC.

DISCUSSION

The expected 5-year survival rate for PDAC is a mere 9%, and although great strides have been made in understanding what genetic events initiate and support tumorigenesis, there has been little progress in the diagnosis, prevention, or treatment of pancreatic cancer (Siegel et al., 2019). In this study, we shed light on a mechanism of regulation of a metabolic enzyme, NADK, which sustains PDAC. Specifically, we show that oncogenic KRAS, the main genetic driver of PDAC, leads to NADK hyperactivation by promoting PKC activation and consequent NADK phosphorylation. NADK hyperactivation in turn powers reductive biosynthesis and maintains a redox homeostasis, thus enabling PDAC growth.

NADK plays a pivotal role in maintaining cellular homeostasis, allowing cells to efficiently adjust their reducing equivalent pools to reflect the abundance of nutrients, energy, reactive oxygen species, and growth factors. In order to ensure homeostasis under physiological and pathological conditions, NADK's activity is regulated by a myriad of factors. NADK is regulated through competitive inhibition by NADPH and NADH, thus putting a break on *de novo* NADP+ synthesis when there is no need for it (Grose et al., 2006; Ohashi et al., 2011). Moreover, Ca^{2+} levels have also been shown to modulate NADK activity through Ca^{2+}/calmodulin-dependent kinase II (CamKII)-dependent phosphorylation of NADK, although the functionality of this phosphorylation remains to be determined, as no change in NADK enzymatic activity was observed after CamKII phosphorylation (Love et al., 2015). In addition to being regulated by the metabolic and redox state of the cell, NADK has recently been shown to be regulated by growth factor signaling through a phosphatidylinositol 3-kinase (PI3K)-dependent and AKT-mediated phosphorylation of three N-terminal serines (Hoxhaj et al., 2019). Our work adds oncogenic KRAS to the growing modes of NADK regulation and demonstrates the important nature of this regulatory circuit for PDAC tumorigenesis.

How broadly applicable can these findings be? *De novo* synthesis of NADP+ is likely to play a role in multiple types of cancer, as it is important for proliferation as well as for redox control. In addition to PDAC, NADK suppression has been shown to be deleterious in different types of cancer including KRAS-driven colon cancer and PI3K-driven breast cancers. Although more work is needed to understand the regulatory circuits that control NADK in other types of cancer, our data add melanoma and lung adenocarcinoma to the growing list of cancers that rely on NADK. On the other hand, uncontrolled NADK activity

can also be deleterious to cells, as it is likely to deplete cellular NAD+ stores and disrupt various cellular processes. Thus, it is likely that the dependence on NADK and consequently the signaling pathways that regulate its activity are defined by the tissue of origin and the genomic drivers, as well as the stage of the tumor.

LIMITATIONS OF STUDY

This study demonstrates that NADK powers antioxidant systems and biosynthesis of nucleotides and lipids. However, it is clear through our supplementation experiments that NADK's role in PDAC goes beyond these aspects of metabolism. More work will be necessary to address additional functions of NADK that can account for its importance to PDAC. This study also does not address the dependency of NADK throughout PDAC formation and progression *in vivo*. It is possible that at different stages of tumorigenesis NADK is important for different aspects of PDAC biology. Finally, although we see that NADK acts downstream of PKC and that NADK silencing impacts PDAC growth, PKC inhibitors have failed in clinical trials for PDAC (Storz, 2015). This opens the possibility that NADK is regulated by other means in PDAC or that PKC inhibition activates a compensatory mechanism that keeps NADK activity on. PKC has been observed to inhibit AKT signaling (Li et al., 2006; Motley et al., 2001), and it is possible that PKC inhibition activates AKT to phosphorylate NADK. In that case, mutation of both PKC and AKT phosphorylation sites would be necessary to achieve greater inhibition of NADK activity.

STAR★METHODS

RESOURCE AVAILABILITY

Lead contact: Further information and requests for resources and reagents should be directed to and will be fulfilled by the Lead Contact, John Blenis (job2064@med.cornell.edu).

Materials availability: All reagents generated in this study are available from the Lead Contact without restriction.

Data and code availability: The published article includes all datasets generated or analyzed during this study. Raw Western Blot data were deposited on Mendeley https://dx.doi.org/10.17632/cwbdnmjmk5.1.

EXPERIMENTAL MODEL AND SUBJECT DETAILS

Cell Lines: PDE human epithelial ductal cells (hTERT-HPNE E6/E7/st) were obtained from the American Type Culture Collection (ATCC), and were cultured according to ATCC specifications. Briefly, they were cultured in low glucose DMEM (GIBCO), 5% FBS (Sigma-Aldrich), 25% INCELL M3:Base F (Thermo Fisher Scientific), 10 ng/mL human rEGF (PeproTech). BxPC3, MIA PaCa-2, and PANC-1 human PDAC cell lines were purchased from ATCC and were grown in high glucose DMEM (GIBCO) supplemented with 10% FBS (Sigma-Aldrich). A-375 and A549 cells were purchased from ATCC and were grown in high glucose DMEM (GIBCO) supplemented with 10% FBS (Sigma-Aldrich). SK-MEL-28 and NCI-H1975 were a gift from Dr. Lewis Cantley's lab and were

grown in high glucose DMEM (GIBCO) supplemented with 10% FBS (Sigma-Aldrich). HEK293T cells were purchased from GenHunter and cultured in high glucose DMEM (GIBCO) supplemented with 10% FBS (Sigma-Aldrich). HEK293A cells were obtained from Thermo Fisher Scientific and were cultured under the same conditions as HEK293T cells. KP MEFs were gifted to us by Dr. Gina DeNicola and were cultured as previously described (DeNicola et al., 2011). Adenoviral Cre (SignaGen Laboratories) was added to cells in culture for 4 days to induce expression of conditional $KRAS^{G12D}$ allele. All cell lines were maintained at 37°C and 5% CO_2. All cell lines were routinely tested for mycoplasma and were at all times mycoplasma negative.

Mice: Female nu/nu athymic mice were purchased from Envigo at the age of 4–6 weeks. Xenograft experiments were started 7–10 days after the mice were received. $Kras^{+/LSL\text{-}G12D}$ C57BL/6 mice were a kind gift from Dr. Lukas Dow, and were immediately used to isolate pancreatic organoids. The nu/nu mice were maintained at Weill Cornell Medicine in compliance with Weill Cornell Medicine Institutional Animal Care and Use Committee protocols.

METHOD DETAILS

Plasmid generation, cloning and mutagenesis: Human NADK cDNA was obtained from Addgene (pWZL-Neo-Myr-Flag, Plasmid 20415) and cloned into the pENTR1A vector (Addgene plasmid 17398) using Gateway PB cloning kit (Life Technologies). NADK cDNA contained c786a mutation in its nucleotide sequence which resulted in N to K amino acid substitution. Mutation was corrected using Quikchange II XL site directed mutagenesis kit (Agilent Technologies). An HA tag was PCR cloned onto the N-terminal end of NADK using primers: forward TAAGCAGTCGACATGTACCCATACGATGTTCCAGATTACGCTATGGAAATGGAACA AGAAAAAATGACCATGAATAA and reverse TGCTTACTCGAGTCATTACTAGCCCTCCTCCTCCTCCTC. HA tagged NADK was then cloned into either pLenti CMV Hygro DEST (Addgene plasmid 17454) or pLenti PGK Hygro DEST (Addgene plasmid 19066) using Gateway LR cloning kit (Life Technologies). NADK unphosphorylatable, phosphomimetic and shRNA-resistant point mutants were generated by site-directed mutagenesis in pENTR1A using the Quikchange II XL site directed mutagenesis kit (Agilent Technologies). pInducer20 (plasmid 44012), pDONR223 GFP (plasmid 15301) and pDONR223 $KRAS^{G12V}$ (plasmid 31200) were all purchased from Addgene. GFP and $KRAS^{G12V}$ were cloned into pIducer20 using Gateway LR cloning kit (Life Technologies). All vectors were sequence verified prior to use.

Generation of stable overexpressing cell lines: pInducer20 GFP and $KRAS^{G12V}$ lentiviruses were produced by co-transfection of HEK293T cells with plasmids encoding psPAX2 (Addgene plasmid 12260), and pMD2.G (Addgene plasmid 12259) using X-tremeGENE HP (Roche) in accordance with the manufacturer's protocol. Media was changed 24 hours post-transfection and the virus harvested after 48 hours, filtered, and used to infect PDE cells in the presence of 8 μg/ml polybrene (Sigma-Aldrich). Selection of resistant colonies was initiated 24 hours later using 1200 μg/ml G418 (Sigma-Aldrich). Cells were induced with 1 μg/ml of doxycycline for 12–48 hours. pLenti viruses were similarly

produced and used to infect PANC-1, MIA PaCa-2, PDE and HEK293A cells. Selection was carried out using 100 μg/ml Hygromycin B (Thermo Fisher).

shRNA mediated silencing: shNADK #1 (TRCN0000037700), shNADK #2 (TRCN0000199808), shNADK #3 (TRCN0000199040), shNadk #1 (TRCN000 0297518), shNadk #2 (TRCN0000278616), shKRAS #1 (TRCN0000369099), and shKRAS #2(TRCN0000033260) were all purchased from Sigma-Aldrich as glycerol stocks. Lentiviruses were produced, and infection was carried out as previously described. One day post infection, PANC-1, MIA PaCa-2, and BxPC3 were selected with 2 μg/mL Puromycin (Sigma-Aldrich) for 24 hours. Blasticidin resistant shRNA constructs were made through ligation of oligos corresponding to the TRCN numbers described above into pLKO.1-blast (Addgene plasmid 26655). Infection of PDE cells with Blasticidin-resistant lentiviral shRNAs and their selection were achieved as previously described. All experiments were carried out 46–96 h post infection. For MIA PaCa-2, rescue experiments were carried out with shNADK hairpins 1 and 3. For PANC-1, rescue experiments were carried out with shKRAS #1 and 2.

siRNA mediated silencing: Mission esiRNA PKC alpha (EHU050821), beta (EHU069171), gamma (EHU034121) and delta (EHU067061) were purchased from Sigma-Aldrich. MIA PaCa-2 cells or PDE cells were transfected in 6 cm plates at 40%–60% confluency. 4 μL (from 20 μM stock) of siRNA and 4 μL Lipofectamine RNAiMAX Transfection Reagent (Thermo Fisher) were diluted in 400 μL Opti-MEM (Life Technologies) prior to transfection of cells. 24–48 h post transfection, cells were starved of serum overnight, and then were collected either for immunoprecipitation or Western Blotting, as previously described.

Cell line treatments: PDE cells were treated with 0–50 μM tert-Butyl hydroperoxide (TBH) for 24–72 h before being harvested for biomass quantification. To induce the phosphorylation of NADK and NADP+ synthesis, PDE, HEK293A, MIA PaCa-2 and PANC-1 cells were treated with 100 ng/ml phorbol 12-myristate 13-acetate (PMA) which activates PKC. Treatments were typically carried out for 20 min-1 h. In some cases, cells were co-treated with 500 nM Sotrastaurin (SOT) for 1 h to inhibit PKC. To check if SOT can inhibit phosphorylation of NADK without PMA induction, PANC-1 cells were treated with 500 nM of SOT alone for 1 h prior to cell lysis IP of NADK. Finally, to see if mutant $KRAS^{G12V}$-induced phosphorylation of NADK can be blunted with SOT, PDE cells carrying inducible $KRAS^{G12V}$ construct were treated with 1 μg/mL of doxycycline for 24 h. For the last hour of induction, 500 nM SOT was added to cells which were then harvested for IP of NADK. Prior to resolving endogenous NADK via Phos-tag, PDE cells were treated with 500 nM insulin for 20 min, 10% serum for 20 min or 100 ng/ml PMA for 20 min. To test the effect of other stimuli on NADK phosphorylation, PDE cells were treated with 5 μM ionomycin for 5 min, 100 ng/ml EGF for 10 min, 100 nM insulin for 10 min, 10% serum for 10 min, 750 μM H_2O_2 for 30 min, or 100 ng/ml PMA for 30 min. Treatments were conducted prior to NADK IP. To determine the contribution of CAMKII to phosphorylation of NADK, PDE cells were co-treated with either 500 nM SOT and 5 μM ionomycin for 5 min or 10 μM KN-93 and 5 μM ionomycin for 5 min following by NADK IP. To test how

other pathways influence phosphorylation of NADK, PDE cells were co-treated with 100 ng/ml PMA and 10 μM S6K inhibitor PF4708671, 2 μM RSK inhibitor BID1870, 2 μM MEK1/2 inhibitor AZD6244, 2 μM AKT inhibitor MK2206,10 μM GSK3 inhibitor CHIR 99021, 2 μM PI3K inhibitor GDC0941, or 250 nm mTOR inhibitor Torin.

Immunoprecipitation: PDE, HEK293A, and PANC-1 cells expressing N-terminally HA tagged WT or mutant NADK were subjected to treatments described above prior to immunoprecipitation. Cells were then lysed in 50 mM Tris HCl pH 7.5, 150 mM NaCl, 0.5% NP40 (IGEPAL, Sigma-Aldrich). 500–1000 ug of protein lysate were incubated with monoclonal anti-HA agarose slurry (Sigma-Aldrich) for 2 hours. Post incubation proteins bound to agarose were washed with lysis buffer 3 times and then eluted in 250 μg/ml HA peptide solution in PBS (Sigma-Aldrich) for 30 min. Purified NADK was resolved using standard or Phos-tag immunoblot. NADK was detected with total anti-NADK antibody, PKC substrate antibody, anti-HA antibody or with custom-made pNADK S64 antibody.

Western blots: Proteins were isolated directly from intact cells via acid extraction using a 10% TCA solution (10% trichloroacetic acid, 25 mM NH_4OAc, 1 mM EDTA, 10 mM Tris HCl pH 8.0). Precipitated proteins were harvested and solubilized in a 0.1 M Tris$HCl pH 11 solution containing 3% SDS. Normalized protein lysates were subjected to SDS-PAGE. Following antibodies were used: NADK (CST 55948S), NADK (Bethyl Laboratories A304–993A), RASG12D (CST 14429S), RASG12V (CST 14412S), RAS (CST 3339S), RAS (CST 3965S), FLAG (MA1–91878-1MG Thermo Fisher), PKC Substrate (CST 6967S), PKA Substrate (CST 9624S), AKT Substrate (CST 10001S), PKC alpha (CST 2056S), PKC delta (CST 2058S), PKC beta (SCBT sc-209), PKC gamma (SCBT sc-211), PKC theta (SCBT sc-212), PKC epsilon (SCBT sc-214), PKC eta (SCBT sc-215), pan-PKC (SCBT sc-17769), HA (SCBT sc-7392), pMARCKS S159/153 (CST 11992S), pMARCKS S152/156 (CST 2741S), pMARCKS S167/170 (CST 8722S), MARCKS (CST 5607S), Vinculin (Sigma-Aldrich V9264), pERK1/2 T202/Y204 (CST 4370L), ERK1/2 (CST 4696S), pAKT T308 (CST 13038S), pAKT S473 (CST 4060L), AKT (CST 4691S), EGFR (CST 2239S), COXIV (CST 4850S), GAPDH (Sigma-Aldrich G8795–200UL), pNADK S64 (Abcam, custom-made) (Batonick et al., 2016; Huang et al., 2016). pNADK S64 custom-made antibody was tested through both NADK knockdown and S64A mutagenesis.

Phos-tag: To detect the phosphorylation of endogenous NADK, cells were lysed in 10 mM Tris HCl pH 8, 1 mM EDTA, 0.5 mM EGTA, 140 mM NaCl, 1% Triton, 0.1% SDS, 0.1% Sodium deoxycholate, and resolved on pre-cast Phos-tag gels (Wako). To detect the phosphorylation of immunoprecipitated NADK, similar Phos-tag technique was employed, but using cell lysis and NADK immunoprecipitation method described in the “Immunoprecipitation” section. In this case, instead of the whole cell lysate, purified NADK was resolved on Phos-tag gels. For PANC-1 shKRAS experiment, cells expressing pLenti NADK construct were used, and the whole cell lysate was resolved. For transfer of phosphorylated proteins to the membrane, the manufacturer’s instructions were followed.

Cell fractionation: To detect the activation of PKC, cells were divided into cytosolic and membrane fractions following PMA treatment (PMA treatments previously described) using

a subcellular protein fractionation kit (Thermo Fisher). Manufacturer's instructions were followed for protein fractionation prior to western blotting.

ROS measurements: CM-H2DCFDA dye (Thermo Fisher) was used to stain for ROS following NADK knockdown in MIA PaCa-2 and PANC-1 cells. Cells were seeded in 96 well plates at 10,000 cells per well. The next day, cells were washed in PBS and incubated with 20 μM DCFDA stain diluted in PBS for 45 min at 37°C. Post staining, cells were washed in PBS again and fluorescence was read at Ex/Em 485/535 nm using Envision plate Reader (Perkin Elmer). For treatment of MIA PaCa-2 cells with 1 mM N-acetyl-L-cysteine (NAC, Sigma-Aldrich), cells were seeded in 96 well plates and NAC was added the next day after seeding. Treatment was carried out for 24 h.

3D colony formation assay in agarose: 6 well plates were coated with a 1:1 ratio of 2 x DMEM (Millipore): 1.2% SeaPlaque Agarose (Lonza). 5,000 of the indicated cells per well were plated in a second layer of agarose (1:1 ratio of 2 x DMEM and 0.7% agarose). The day after seeding, 0.5 mL of 1 x DMEM (GIBCO) with appropriate selection antibiotic was added per well. Selection antibiotics were also added to the top and bottom layers of agarose. Cells were fed with 0.5 mL of media once a week for 4–6 weeks. Where indicated, 2 mM N-acetyl-L-cysteine (NAC, Sigma-Aldrich), or 5 mg/L nucleosides (EmbryoMax, EMD Millipore), or 12 μg/ml low density lipoprotein (LDL, Sigma-Aldrich) and 50 μM oleate (Sigma-Aldrich) alone or in combination were added to MIA PaCa-2 shNADK cell colonies in 0.5 mL 1 × DMEM every 3 days. Lipids (LDL and oleate), NAC or nucleosides alone or all three in combination were also included in the top and bottom layers of agarose.

2D growth curve: 70,000 of the indicated cells were plated per well in 6 well plates. Every day cells were trypsinized and counted. Growth rate was calculated as fold change in cell number relative to 24 hours.

Biomass quantification: Cells in 2D culture were fixed in 4% PFA for 20 min then stained with 0.1% Crystal violet solution for 20 min. To quantify cellular biomass, crystal violet stain was eluted with 100% methanol and the absorbance was measured at 590 nm using an Envision Plate Reader (Perkin Elmer). To visualize and quantify 3D colonies, cells were stained in 0.005% Crystal violet/10% Ethanol aqueous solution for 3 hours. Plates were de-stained in water overnight and colonies were counted by eye.

Xenograft assays: Flanks of athymic nu/nu mice were subcutaneously injected with 1.5 × 10^6 of MIA PaCa-2 shNADK or shNT (non-targeting) infected cells in PBS at 1:1 with Growth Factor Reduced Matrigel (Corning) in 100 μl. PANC-1 cells were first infected with either pLenti GFP, pLenti HA-NADK WT or S46A/S64A mutant. Cells were split into 100 μg/ml Hygromycin B (Thermo Fisher) 24 h post infection. Cells were then selected for 24h in Hygromycin B. Hygromycin B was washed out, and cells were infected with either shNT or shNADK #2 (TRCN0000199808). Cells were selected in Puromycin (Sigma-Aldrich) for 3 days before being injected into mice, as previously described. Tumors were measured weekly with calipers and the volume was calculated according to the formula (W^2 × L)/2. On week 5 post injection, mice were sacrificed and tumors were dissected out for photographing.

Murine pancreatic ductal organoid culture: For isolation and culture of normal pancreatic organoids, we followed the protocol supplied by Huch et al., 2013. Briefly, normal pancreatic ducts were isolated from $Kras^{+/LSL\text{-}G12D}$ C57BL/6 8 to12-week-old mice and seeded into Growth Factor Reduced Matrigel (Corning). Once Matrigel solidified, Advanced DMEM/F12 media (Thermo Fisher) was added containing 15 mM HEPES, 1% Pen/Strep (Thermo Fisher), 2 mM glutamine (Sigma-Aldrich), B27 supplement (1x, Invitrogen), 1.25 mM N-acetylcysteine (Sigma-Aldrich), 10 nM Gastrin I (Sigma-Aldrich), 50 ng/ml murine EGF (Peprotech), 500 ng/ml murine RSPO (Peprotech), 100 ng/ml murine Noggin (Peprotech), 100 ng/ml human FGF-10 (Peprotech), and 10 mM Nicotinamide (Sigma-Aldrich). To induce $KRAS^{G12D}$ expression, Adenoviral Cre (SignaGen Laboratories) was added directly into Matrigel during organoid passaging. To silence p53, organoids were infected with lentivirus carrying CRISPR/Cas9 sgRNA gifted to us by Dr. Lukas Dow. Prior to lentiviral infection, organoids were dissociated using 200 μL TrypLE™ express (Thermo Fisher) for 5 min at 37°C. Then, organoids were resuspended in 150 μL of Advanced DMEM/F12 full culture media and 150 μL lentivirus-containing media with 8 μg/ml polybrene (Sigma-Aldrich), 5 μM CHIR99021 (Selleck Chemicals) and 10 μM Y27632 (Sigma-Aldrich) in 48 well plates. Plates were centrifuged at 600 g for 60 min at 32°C to spinoculate. Post centrifugation, plates were incubated at 37°C for 4 h, and organoids were spun out of the infection media and plated in Matrigel. Experiments were carried out approximately 1–2 weeks following transformation. To assay the effect of Nadk silencing on organoids, organoids were subjected to lentiviral infection with shNT, shNadk #1 or shNadk #2 as described above. To select shRNA-containing organoids, full Advanced DMEM/F12 culture media was supplemented with 2 μg/ml puromycin (Sigma-Aldrich). Selection was carried out for one week, with two organoid passages. To quantify the organoid number post infection and selection, equal number of organoids was plated in 50 μL of Matrigel for 24h, following which, organoids were counted by eye. To check the efficiency of Nadk knockdown, organoids were harvested using Cell Recovery Solution (Corning) according to the manufacturer's protocol. After recovery, organoids were lysed in RIPA or NP-40 lysis buffer as previously described and resolved on immunoblot.

NADK purification: HEK293A cells expressing HA-tagged WT, S46A or S64A NADK were starved of serum overnight and then stimulated with 100 ng/ml PMA for 1 h. Cells were lysed in 50 mM Tris pH 7.5, 150 mM NaCl, 1 mM EGTA, 1 mM EDTA, 0.5% NP40, 2 mM DTT. Lysates were incubated with anti-HA agarose (Sigma-Aldrich) for 4 h. Agarose was washed first in Buffer 1 consisting of 50 mM Tris pH 8.0, 1 M NaCl, 0.03% Brij-35, 0.1 mM EGTA, 2 mM DTT. Then, agarose was washed in Buffer 2 consisting of 50 mM Tris pH 8.0, 150 mM NaCl, 0.03% Brij-35, 0.1 mM EGTA. Finally, agarose was washed in Buffer 3 consisting of 50 mM Tris pH 8.0, 150 mM NaCl. Bound proteins were eluted with 250 μg/ml HA peptide diluted in 50 mM Tris pH 8.0, 150 mM NaCl. Eluates were diluted in Buffer 2 and subsequently concentrated using Amicon Ultra-4 Centrifugal Filter Units with Ultracel-10 membrane (Millipore-Sigma).

***In vitro* NADK activity assay:** 0.2 μg of purified WT, S46A or S64A NADK were assayed for their ability to form NADP+ using previously described methodologies (Lerner et al., 2001; Pollak et al., 2007; Love et al., 2015). Assay buffer contained 5 mM Adenosine

5′-triphosphate magnesium salt (ATP, Sigma-Aldrich), 2 mM Glucose 6-phosphate (Sigma-Aldrich), 0, 2.5, 5 and 10 mM beta-Nicotinamide adenine dinucleotide sodium salt (NAD+, Sigma-Aldrich), 10 mM $MgCl_2$, 100 mM Tris$HCl pH 8 and 25 ng human glucose 6-phosphate dehydrogenase (G6PD, Sigma-Aldrich). The assay was carried out in 96 well plates measuring the change in absorbance over time at 340 nm as NADP+ produced by NADK got converted into NADPH by G6PD.

***In vitro* phosphorylation of NADK by PKC:** NADK was purified via immunoprecipitation, as previously described, from serum starved PDE or HEK293A cells with one modification. Prior to elution from the HA beads, NADK was subjected to phosphorylation by PKC. Reaction was carried out in buffer containing 25 mM MOPS pH 7.2, 12.5 mM β-glycerol-phosphate, 25 mM MgCl2, 5 mM EGTA, 2 mM EDTA, 0.25 mM DTT, 50 μM ATP (SignalChem), 1 x PKC lipid activator (SignalChem), 5 ng/μl BSA, 0.5% glycerol, 100 ng PKC (SignalChem). Prior to phosphorylation, beads containing bound NADK were washed once with 25 mM MOPS pH 7.2, 12.5 mM β-glycerol-phosphate, 25 mM MgCl2, 5 mM EGTA, 2 mM EDTA. Reaction was carried out for 30 min at 30°C. To show the specificity of phosphorylation, 250 nM SOT was co-incubated with PKC. Reaction was terminated by washing the beads with the immunoprecipitation buffer containing 50 mM Tris HCl pH 7.5, 150 mM NaCl, 0.5% NP40. NADK was then eluted from beads as previously described before being resolved via immunoblot. Phosphorylation on NADK was visualized as previously described using Phos-tag and phospho-specific antibodies.

LC-MS/MS-based phospho-peptide analyses: WT or mutant NADK were immunoprecipitated from PDE and HEK293A cells, as previously described. Cells were starved of serum overnight and treated with PMA or co-treated with PMA and SOT for an hour, as previously described. PDE cells were also starved of serum overnight prior to inducible expression of GFP or $KRAS^{G12V}$, as previously described, prior to immunoprecipitation. Purified NADK proteins were run on a polyacrylamide gel and NADK protein bands were visualized via staining the gel with SimplyBlue Safe-Stain (Thermo Fisher) according to manufacturer's instructions. Following de-staining with water, NADK protein bands were excised from the gel with a razor. In-gel digests were performed using 10 ng/μl trypsin in 50 mM ammonium bicarbonate after excising and destaining Coomassie stained bands. Extracted peptides were desalted using hand-packed C18 STAGE Tips (Rappsilber et al., 2003). Peptides were eluted with 50 μL of 70% acetonitrile (ACN), 1% formic acid (FA) into glass vial inserts and dried in a speed-vac centrifugal evaporator. Samples were re-suspended in 10 μL of 5% (FA) and analyzed twice, using 1 μL each for a data-dependent acquisition (DDA) method, and then a targeted parallel reaction monitoring method (PRM). Both methods used an identical 20 min, two-stage gradient of 1) 5%–13% buffer B (0.1% FA in ACN) for 10 min followed by 2) 13%–25% buffer B for 10 min. In the DDA method, precursor scans were performed in the orbitrap at 60K resolution with AGC target = 400,000 and a maximum ion accumulation time of 50 ms. Using a cycle time of 1 s, the most abundant ions were selected for HCD fragmentation and scanned in the orbitrap at 30,000 resolution with an AGC target = 50,000 and a maximum ion accumulation time = 54 ms. Dynamic exclusion was set at 5 s in order to sample each peak more than once. In the PRM method, no MS1 scans were collected. Instead, the instrument was directed to collect

MS2 spectra for targeted precursor masses corresponding to different NADK peptides that were identified in the DDA method (listed below), throughout the entire run. Note that different phosphoforms of equal mass are represented by only a single entry. This provides high-density fragment ion intensities used to identify and quantify specific phosphoforms based on unique product ions. DDA runs were searched using SEQUEST (version 28 revision 13) against a composite database containing all Swiss-Prot reviewed human protein sequences (20,193 target sequences, downloaded from https://www.uniprot.org/, March 18, 2016) supplemented with mutant NADK sequences and the reversed complement sequences, using the following parameters: a precursor mass tolerance of ± 20 ppm; 0.03 Da product ion mass tolerance; tryptic digestion without prohibition on +1 proline; up to two missed cleavages; a static modification of carbamidomethylation on cysteine (+57.0214); dynamic modifications of methionine oxidation (+15.9949) and phosphorylation on serine, threonine, and tyrosine (+79.9663). Peptide spectral matches (PSMs) were filtered to 1% FDR using the target-decoy strategy (Elias and Gygi, 2007) combined with linear discriminant analysis (LDA) (Huttlin et al., 2010) using several different parameters including Xcorr, DCn', precursor mass error, observed ion charge state, and predicted solution charge state. Linear discriminant models were calculated for each LC-MS/MS run using peptide matches to forward and reversed protein sequences as positive and negative training data. PSMs within each run were sorted in descending order by discriminant score and filtered to a 1% FDR as revealed by the number of decoy sequences remaining in the dataset. DDA search results were used to generate spectral libraries in Skyline (Version 4.2.0.19072; MacLean et al., 2010). Phosphorylation site assignment was performed manually in Skyline using phosphorylation site-determining ions observed in the PRM runs as follows. Analysis of WT NADK revealed three prominent peaks corresponding to singly phosphorylated forms of SLSASPALGSTK. pS46 (SLSASPALGSTK) was identified as the latest eluting peak (z = 2+, m/z = 599.7894) by site specific ions b2+ (pSL-, 281.0897) and y10+ (-SASPALGSTK, 918.4891). No single fragment ions are unique to pS48 and pS50. To identify peaks corresponding to these sites, we looked for the co-occurrence of fragments, which together can uniquely assign a particular phosphoform to a single peak. For pS48, the b2+ ion (SL-, 201.1234) is common to pS48, pS50, pS55, and pT56. The b3+ ion (SLpS-, 368.1217) is common only to pS46 and pS48. These two ions elute in multiple peaks, but were found together only in the peak eluting at 19.8 min and corresponding to pS48. Similarly, for pS50, y7+ (-PALGSTK, 673.3879) is common to pS46, pS48, pS50 and elutes in three peaks. The y8+ ion (-pSPALGSTK, 840.3863) is common to pS50, pS55, and pS56. Ions y7+ and y8+ co-elute in only one peak at 19.1 min, corresponding to pS50. Similar analysis of phosphorylation site mutant NADK proteins recapitulated the above assignments as well as the quantitative findings. The S46A mutant resulted in only two prominent peaks with mass equal to the singly phosphorylated peptide, neither regulated by PMA. All other single site mutants tested (S48A, S50A, S55A) generated two peaks, one upregulated by PMA, one not. Phosphorylation site quantification was derived from the integrated area under the curve of precursor ion peaks from the corresponding DDA runs in Skyline.

Total NAD(P)+ and NAD(P)H measurements: For shNADK expressing MIA PaCa-2 and BxPC3 cells and for shKRAS expressing PANC-1 cells, NAD(P)+ and NAD(P)H levels were obtained from the targeted metabolomics analysis (described below). For $KRAS^{G12V}$

expressing PDE cells, NAD(P)+ and NAD(P)H measurements were obtained using the extraction methodology employed in isotope tracing experiments (described below). For all other experiments and to support the findings from the above experiments, a luciferase-based method, NADP/NADPH-Glo Assay (Promega), was used to measure NAD(P)+ and NAD(P)H according to manufacturer's instructions (Hoxhaj et al., 2019).

Isotope tracing of *de novo* NADP+ generation: All cells were grown in 6 cm plates to 60%–80% confluency. PDE cells expressing inducible $KRAS^{G12V}$ construct were starved of serum for 24 h. 8–10 h post starvation, cells were washed in PBS and 1 μg/mL of doxycycline and 32 μM [2,4,5,6-^{2}H]nicotinamide ([^{2}H]NAM, Cambridge Isotope Laboratories) were added in serum free, NAM free media. 15 h post labeling and $KRAS^{G12V}$ induction, cells were harvested. PANC-1 and MIA PaCa-2 cells were starved of serum for 24 h. 8–10 h post starvation, cells were washed in PBS and 32 μM [^{2}H]NAM was added in serum free, NAM free media. 15 h post labeling, cells were treated with 100 ng/ml PMA for 1 h or co-treated with 100 ng/ml PMA and 500 nM SOT for 1 h. Cells were then harvested. PDE cells expressing NADK shRNA and WT or S46A/S64A NADK cDNA were starved of serum for 24 h. 8–10 h post starvation, cells were washed in PBS and 32 μM [^{2}H]NAM was added in serum free, NAM free media. 15 h post labeling, cells were treated with 100 ng/ml PMA for 1 h. To compare NADP+ synthesis levels in the panel of cell lines, PANC-1, MIA PaCa-2, A-375, SK-MEL-28, A549, and NCI-H1975 were grown in NAM free media with 10% dialyzed serum (Sigma-Aldrich) and 32 μM [^{2}H]NAM for 2 h prior to harvesting. To harvest cells, media was removed and replaced with 1 mL of ice-cold 40% MeOH/40% acetonitrile/20% water/0.5% formic acid. Cells were incubated in the solution for 30 s, following which 80 μL of 2M NH_4HCO_3 were added to cells to neutralize. Cells were moved to −20°C for 30 min. After the incubation, cells were scraped off the frozen plates and placed into Eppendorf tubes. Tubes were placed on dry ice for 5 min and then spun down in a microfuge at 16,000 r*cf*. for 10 minutes at 4°C. Supernatants were collected in a fresh tube and frozen at −80°C until further processing. The supernatants were centrifuged at 16,000 g for 20 minutes to remove any residual debris before analysis. Supernatants were analyzed within 24 hours by liquid chromatography coupled to a mass spectrometer (LC-MS). The LC–MS method involved hydrophilic interaction chromatography (HILIC) coupled to the Q Exactive PLUS mass spectrometer (Thermo Scientific). The LC separation was performed on a XBridge BEH Amide column (150 mm 3 2.1 mm, 2.5 mm particle size, Waters, Milford, MA). Solvent A is 95%: 5% H2O: acetonitrile with 20 mM ammonium bicarbonate, and solvent B is acetonitrile. The gradient was 0 min, 85% B; 2 min, 85% B; 3 min, 80% B; 5 min, 80% B; 6 min, 75% B; 7 min, 75% B; 8 min, 70% B; 9 min, 70% B; 10 min, 50% B; 12 min, 50% B; 13 min, 25% B; 16 min, 25% B; 18 min, 0% B; 23 min, 0% B; 24 min, 85% B; 30 min, 85% B. Other LC parameters are: flow rate 150 ml/min, column temperature 25°C, injection volume 10 μL and autosampler temperature was 5°C. The mass spectrometer was operated in both negative and positive ion mode for the detection of metabolites. Other MS parameters are: resolution of 140,000 at m/z 200, automatic gain control (AGC) target at 3e6, maximum injection time of 30 ms and scan range of m/z 75–1000. Data were analyzed via the MAVEN software, and all isotope labeling patterns were corrected for natural ^{13}C abundance using AccuCor (Su et. al., 2017). Tracer incorporation into NAD+, NADH and

NADPH were also measured using experimental methods described in this section. When normalization was required due to variation in cell number in between samples, the original data were normalized to protein content.

Targeted metabolomics: Polar metabolites were extracted from BxPC3, PANC-1 and MIA PaCa-2 cells using 80% (v/v) aqueous methanol. Cells were 60%–80% confluent in 6cm plates prior to extraction, and extraction was carried out as previously described (Yuan et al., 2012). Targeted liquid chromatography-tandem mass spectrometry (LC-MS/MS) was performed using a 5500 QTRAPtriple quadrupole mass spectrometer (AB/SCIEX) coupled to a Prominence UFLC HPLC system (Shimadzu) with Amide HILIC chromatography (Waters). Data were acquired in selected reaction monitoring (SRM) mode using positive/negative ion polarity switching for steady-state polar profiling of greater than 260 molecules. Peak areas from the total ion current for eachmetabolite SRM transition were integrated using MultiQuant v2.0 software (AB/SCIEX). The original data was normalized to the mean of the entire metabolome in each sample. Statistical analysis of the data was carried out using MetaboAnalyst, a free online software for the analysis of metabolomic experiments (https://www.metaboanalyst.ca/).

Lipidomics: BxPC3 and MIA PaCa-2 cells infected with shNADK hairpins were grown to 60%–80% confluency on 6 cm plates. Cells were washed with PBS, placed into 1ml of 90% methanol/0.3 M KOH and scraped into a glass vial (Kamphorst et al., 2013). Glass vials were heated at 80°C for 1 h. 100 μL of formic acid (Sigma-Aldrich) were added to acidify. Samples were vortexed and then 1 mL of hexane (VWR) was added to extract lipids. Samples were vortexed again and then the top layer was moved to a new vial. The last step was done twice. Lipids in hexane were dried in a speed vac and stored at −80°C. Dried samples were dissolved in 1 mL of acetonitrile: methanol (1:1, v/v) solution for LC-MS analysis. Separation was performed via reverse-phase-ion-pairing chromatography on a C8 column coupled to negative-ion mode, full-scan LC-MS at 1-Hz scan time and 100,000 resolving power (stand-alone orbitrap; Thermo Scientific). The original data were was normalized to the protein content of each sample. To get the idea of the overall fatty acid content for each cell line, the mean of all fatty acids was calculated.

QUANTIFICATION AND STATISTICAL ANALYSIS

Data analyses were performed using GraphPad Prism8. A two-tailed paired Student's t test was used to determine significance when two conditions were compared. For experiments with more than two conditions a one-way ANOVA was used. In both cases values of $p < 0.05$ were considered significant. Data are shown as the mean ± SEM (standard error of the mean). Data representative of three independent experiments are shown.

Supplementary Material

Refer to Web version on PubMed Central for supplementary material.

ACKNOWLEDGMENTS

We are grateful to the Blenis and Cantley lab members for helpful discussions on the project. We are also thankful to Dr. Gina Lee and Adam Rosenzweig for technical assistance. We are grateful to Dr. Gerta Hoxhaj for technical advice and Dr. Brendan Manning for the NADK lentiviral constructs. We thank Dr. Gina DeNicola for kindly gifting us KP MEFs. We thank Dr. Lukas Dow for $Kras^{+/LSL\text{-}G12D}$ mice and for Tp53 CRISPR-Cas9 sgRNA lentivirus and Dr. Maria Paz Zafra Martin for technical advice on organoids. T.S. was supported by the NIH F31 pre-doctoral fellowship 1F31CA220750-01. A.P.G. was supported by a Susan G. Komen Postdoctoral Fellowship and a Pathway to Independence Award from NCI (K99CA218686). M.R.M. is supported by both the Hanna H. Gray Fellows Program of the Howard Hughes Medical Institute and the Postdoctoral Enrichment Program (PDEP) of the Burroughs Welcome Fund. This research was supported by NIH grants RO1GM51405 and RO1CA46595 to J.B.

REFERENCES

Batonick M, Holland EG, Busygina V, Alderman D, Kay BK, Weiner MP, and Kiss MM (2016). Platform for high-throughput antibody selection using synthetically-designed antibody libraries. N. Biotechnol 33, 565–573. [PubMed: 26607994]

Commisso C, Davidson SM, Soydaner-Azeloglu RG, Parker SJ, Kamphorst JJ, Hackett S, Grabocka E, Nofal M, Drebin JA, Thompson CB, et al. (2013). Macropinocytosis of protein is an amino acid supply route in Ras-transformed cells. Nature 497, 633–637. [PubMed: 23665962]

DeNicola GM, Karreth FA, Humpton TJ, Gopinathan A, Wei C, Frese K, Mangal D, Yu KH, Yeo CJ, Calhoun ES, et al. (2011). Oncogene-induced Nrf2 transcription promotes ROS detoxification and tumorigenesis. Nature 475, 106–109. [PubMed: 21734707]

DeNicola GM, Chen PH, Mullarky E, Sudderth JA, Hu Z, Wu D, Tang H, Xie Y, Asara JM, Huffman KE, et al. (2015). NRF2 regulates serine biosynthesis in non-small cell lung cancer. Nat. Genet 47, 1475–1481. [PubMed: 26482881]

Elias JE, and Gygi SP (2007). Target-decoy search strategy for increased confidence in large-scale protein identifications by mass spectrometry. Nat. Methods 4, 207–214. [PubMed: 17327847]

Eng JK, McCormack AL, and Yates JR (1994). An approach to correlate tandem mass spectral data of peptides with amino acid sequences in a protein database. J. Am. Soc. Mass Spectrom. 5, 976–989. [PubMed: 24226387]

Grose JH, Joss L, Velick SF, and Roth JR (2006). Evidence that feedback inhibition of NAD kinase controls responses to oxidative stress. Proc. Natl. Acad. Sci. USA 103, 7601–7606. [PubMed: 16682646]

Hoxhaj G, Ben-Sahra I, Lockwood SE, Timson RC, Byles V, Henning GT, Gao P, Selfors LM, Asara JM, and Manning BD (2019). Direct stimulation of $NADP^+$ synthesis through Akt-mediated phosphorylation of NAD kinase. Science 363, 1088–1092. [PubMed: 30846598]

Huang R, Kiss MM, Batonick M, Weiner MP, and Kay BK (2016). Generating recombinant antibodies to membrane proteins through phage display. Antibodies (Basel) 5, 11. [PubMed: 31557992]

Huch M, Bonfanti P, Boj SF, Sato T, Loomans CJ, van de Wetering M, Sojoodi M, Li VS, Schuijers J, Gracanin A, et al. (2013). Unlimited in vitro expansion of adult bi-potent pancreas progenitors through the Lgr5/R-spondin axis. EMBO J. 32, 2708–2721. [PubMed: 24045232]

Huttlin EL, Jedrychowski MP, Elias JE, Goswami T, Rad R, Beausoleil SA, Villén J, Haas W, Sowa ME, and Gygi SP (2010). A tissue-specific atlas of mouse protein phosphorylation and expression. Cell 143, 1174–1189. [PubMed: 21183079]

Kamphorst JJ, Cross JR, Fan J, de Stanchina E, Mathew R, White EP, Thompson CB, and Rabinowitz JD (2013). Hypoxic and Ras-transformed cells support growth by scavenging unsaturated fatty acids from lysophospholipids. Proc. Natl. Acad. Sci. USA 110, 8882–8887. [PubMed: 23671091]

Lerner F, Niere M, Ludwig A, and Ziegler M (2001). Structural and functional characterization of human NAD kinase. Biochem. Biophys. Res. Commun 288, 69–74. [PubMed: 11594753]

Li L, Sampat K, Hu N, Zakari J, and Yuspa SH (2006). Protein kinase C negatively regulates Akt activity and modifies UVC-induced apoptosis in mouse keratinocytes. J. Biol. Chem 281, 3237–3243. [PubMed: 16338928]

Liu L, Su X, Quinn WJ 3rd, Hui S, Krukenberg K, Frederick DW, Redpath P, Zhan L, Chellappa K, White E, et al. (2018). Quantitative analysis of NAD synthesis-breakdown fluxes. Cell Metab. 27, 1067–1080.e5. [PubMed: 29685734]

Love NR, Pollak N, Dölle C, Niere M, Chen Y, Oliveri P, Amaya E, Patel S, and Ziegler M (2015). NAD kinase controls animal NADP biosynthesis and is modulated via evolutionarily divergent calmodulin-dependent mechanisms. Proc. Natl. Acad. Sci. USA 112, 1386–1391. [PubMed: 25605906]

MacLean B, Tomazela DM, Shulman N, Chambers M, Finney GL, Frewen B, Kern R, Tabb DL, Liebler DC, and MacCoss MJ (2010). Skyline: an open source document editor for creating and analyzing targeted proteomics experiments. Bioinformatics 26, 966–968. [PubMed: 20147306]

Motley ED, Kabir SM, Eguchi K, Hicks AL, Gardner CD, Reynolds CM, Frank GD, and Eguchi S (2001). Protein kinase C inhibits insulin-induced Akt activation in vascular smooth muscle cells. Cell. Mol. Biol 47, 1059–1062. [PubMed: 11785657]

Ohashi K, Kawai S, Koshimizu M, and Murata K (2011). NADPH regulates human NAD kinase, a $NADP^+$-biosynthetic enzyme. Mol. Cell. Biochem 355, 57–64. [PubMed: 21526340]

Palm W, Park Y, Wright K, Pavlova NN, Tuveson DA, and Thompson CB (2015). The utilization of extracellular proteins as nutrients is suppressed by mTORC1. Cell 162, 259–270. [PubMed: 26144316]

Pollak N, Niere M, and Ziegler M (2007). NAD kinase levels control the NADPH concentration in human cells. J. Biol. Chem 282, 33562–33571. [PubMed: 17855339]

Rappsilber J, Ishihama Y, and Mann M (2003). Stop and go extraction tips for matrix-assisted laser desorption/ionization, nanoelectrospray, and LC/MS sample pretreatment in proteomics. Anal. Chem 75, 663–670. [PubMed: 12585499]

Santana-Codina N, Roeth AA, Zhang Y, Yang A, Mashadova O, Asara JM, Wang X, Bronson RT, Lyssiotis CA, Ying H, and Kimmelman AC (2018). Oncogenic KRAS supports pancreatic cancer through regulation of nucleotide synthesis. Nat. Commun 9, 4945. [PubMed: 30470748]

Siegel RL, Miller KD, and Jemal A (2019). Cancer statistics, 2019. CA Cancer J. Clin 69, 7–34. [PubMed: 30620402]

Son J, Lyssiotis CA, Ying H, Wang X, Hua S, Ligorio M, Perera RM, Ferrone CR, Mullarky E, Shyh-Chang N, et al. (2013). Glutamine supports pancreatic cancer growth through a KRAS-regulated metabolic pathway. Nature 496, 101–105. [PubMed: 23535601]

Storz P (2015). Targeting protein kinase C subtypes in pancreatic cancer. Expert Rev. Anticancer Ther. 15, 433–438. [PubMed: 25604078]

Su X, Lu W, and Rabinowitz JD (2017). Metabolite spectral accuracy on orbitraps. Anal. Chem 89, 5940–5948. [PubMed: 28471646]

Tsang YH, Dogruluk T, Tedeschi PM, Wardwell-Ozgo J, Lu H, Espitia M, Nair N, Minelli R, Chong Z, Chen F, et al. (2016). Functional annotation of rare gene aberration drivers of pancreatic cancer. Nat. Commun 7, 10500. [PubMed: 26806015]

Yau EH, Kummetha IR, Lichinchi G, Tang R, Zhang Y, and Rana TM (2017). Genome-wide CRISPR screen for essential cell growth mediators in mutant KRAS colorectal cancers. Cancer Res. 77, 6330–6339. [PubMed: 28954733]

Ying W (2008). NAD+/NADH and NADP+/NADPH in cellular functions and cell death: regulation and biological consequences. Antioxid. Redox Signal. 10, 179–206. [PubMed: 18020963]

Ying H, Kimmelman AC, Lyssiotis CA, Hua S, Chu GC, Fletcher-Sananikone E, Locasale JW, Son J, Zhang H, Coloff JL, et al. (2012). Oncogenic Kras maintains pancreatic tumors through regulation of anabolic glucose metabolism. Cell 149, 656–670. [PubMed: 22541435]

Yuan M, Breitkopf SB, Yang X, and Asara JM (2012). A positive/negative ion-switching, targeted mass spectrometry-based metabolomics platform for bodily fluids, cells, and fresh and fixed tissue. Nat. Protoc 7, 872–881. [PubMed: 22498707]

Highlights

- *De novo* NADP+ synthesis is increased in KRAS mutant PDAC cells
- NAD+ kinase (NADK) mediates the *de novo* synthesis
- NADK becomes phosphorylated downstream of mutant KRAS and PKCs alpha and delta
- NADP+ synthesis powers anabolic and antioxidant systems

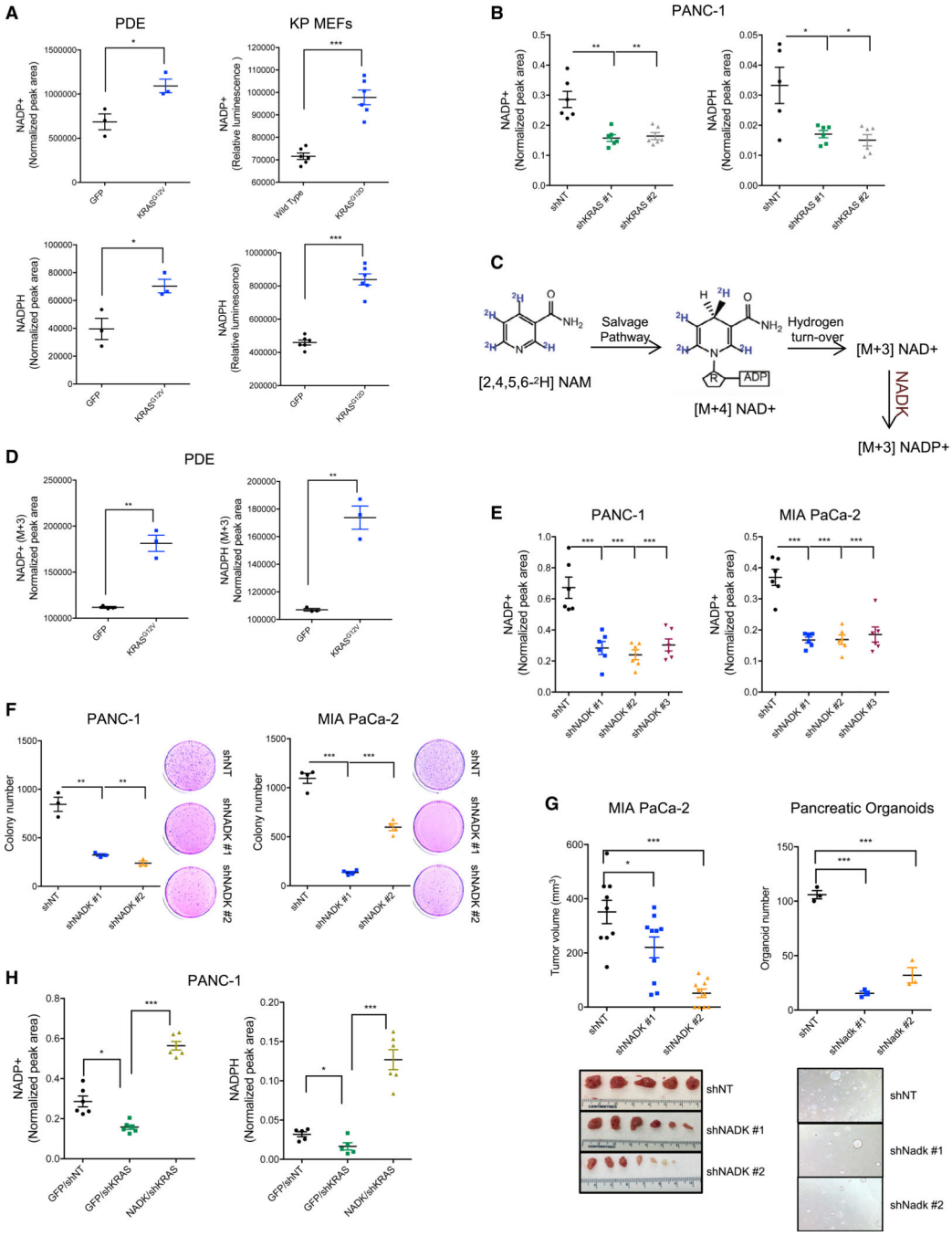

Figure 1. NADK is critical for NADP(H) maintenance in PDAC

(A) Relative NADP(H) levels in pancreatic ductal epithelial cells (PDEs) expressing an ectopic $KRAS^{G12V}$ construct for 24 h and relative NADP(H) levels in mouse embryonic fibroblasts (MEFs) expressing $KRAS^{G12D}$ allele for 4 days. n ≥ 3. For this and further experiments *p < 0.05, **p < 0.01, ***p < 0.001 and error bars represent ± SEM.

(B) Relative NADP(H) levels in PANC-1 cells upon KRAS knockdown by short hairpin RNAs (shRNAs). n ≥ 5.

(C) Schematic of the tracing experiment shown in (D).

(D) Labeling of NADP+ and NADPH from [2,4,5,6-^{2}H]nicotinamide, [^{2}H]NAM, in PDEs expressing KRAS^{G12V} for 24h. n = 3.
(E) Relative NADP+ levels in PANC-1 and MIA PaCa-2 cells upon NADK knockdown by shRNAs. n = 6.
(F) Colony-forming capacity in MIA PaCa-2 and PANC-1 cells upon NADK knockdown by shRNAs. n ≥ 3.
(G) Tumor size of MIA PaCa-2 xenografts (N ≥ 9) upon NADK knockdown and pancreatic ductal organoid number (p53 KO, Kras^{G12D}) upon Nadk knockdown. n = 3.
(H) Relative NADP(H) levels in PANC-1 cells following KRAS knockdown and NADK overexpression. n ≥5.

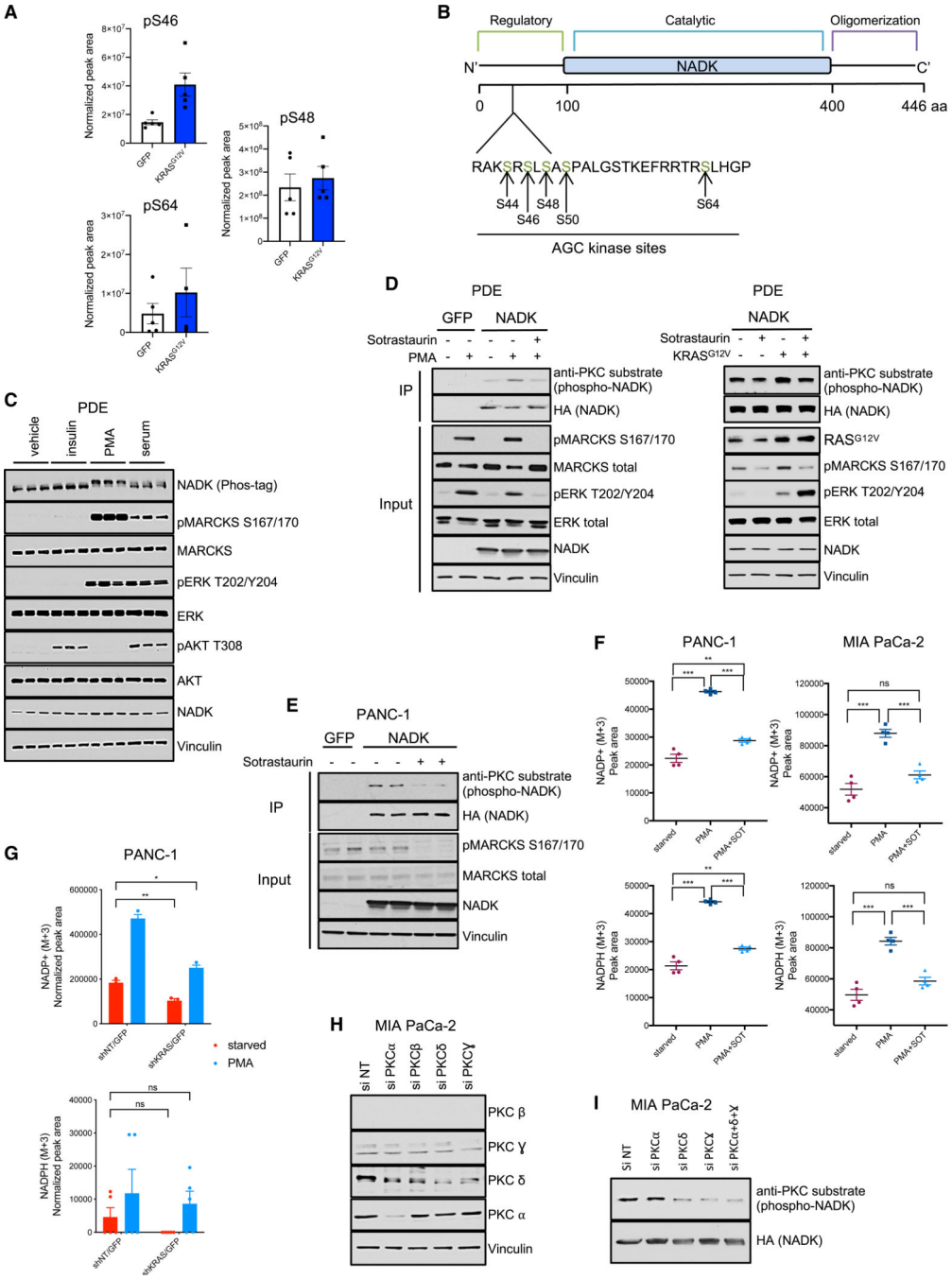

Figure 2. NADK is regulated by KRAS through PKC

(A) Relative peak area of indicated NADK phosphorylation sites detected by LC-MS/MS after overnight serum starvation and inducible $KRAS^{G12V}$ or GFP expression for 2 h in PDEs. $n \geq 3$.

(B) Schematic of NADK domains and putative phosphorylation sites.

(C) Endogenous NADK band shift as observed by Phos-tag immunoblot, following overnight serum starvation and subsequent stimulation with 500 nM insulin, 100 ng/ml PMA, or 10% serum for 20 min in PDEs. n = 3.

(D) Immunoblot of NADK immunoprecipitation (IP) and detection with PKC substrate antibody. PDEs were serum starved overnight followed by 1 h 100 ng/ml PMA treatment or 15-h inducible $KRAS^{G12V}$ expression, with 1-h co-treatment with 500 nM PKC inhibitor Sotrastaurin (SOT) where indicated. n = 3.

(E) Immunoblot of NADK IP and detection with PKC substrate antibody following 1-h treatment with 500 nM SOT in PANC-1 cells. n = 3.

(F) Labeling of NADP+ and NADPH from [^{2}H]NAM. PANC-1 and MIA PaCa-2 cells were serum starved overnight and then treated with 1 h 100 ng/ml PMA and ±500 nM SOT. n = 4.

(G) Labeling of NADP+ and NADPH from [^{2}H]NAM. PANC-1 cells, expressing ±shKRAS, were serum starved overnight followed by 1-h treatment with 100 ng/ml PMA or vehicle control. n = 3.

(H) Immunoblot of MIA PaCa-2 for the indicated PKCs after treatment with isoform-specific PKC siRNAs. n = 3.

(I) Immunoblot of NADK IP and detection with PKC substrate antibody following treatment with the indicated isoform-specific PKC siRNAs in MIA PaCa-2. n= 3.

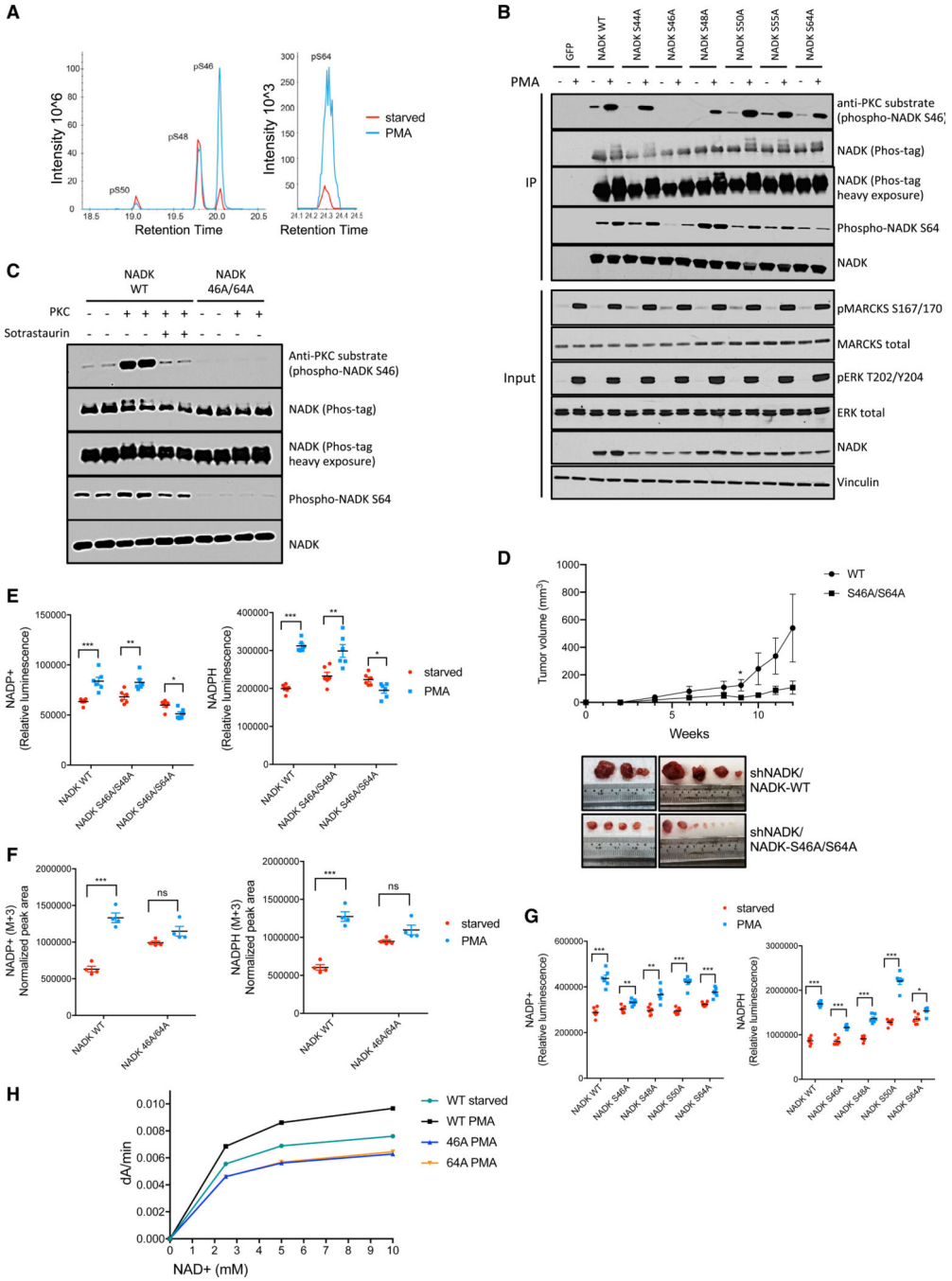

Figure 3. PKC phosphorylates NADK serines 46 and 64 to mediate its activity

(A) Intensity associated with the indicated NADK phosphorylation site detected by LC-MS/MS following overnight serum starvation and 1-h 100 ng/ml PMA treatment in PDEs. n = 3.

(B) Validation of MS findings by Phos-tag and immunoblot with PKC substrate antibody and phopsho-NADK S64 antibody in PDEs treated with PMA as previously described in (A). n = 3.

(C) NADK immunoblot of an *in vitro* kinase assay of PKC phosphorylation of NADK ± 250 nM SOT. n = 3.

(D) Tumor size of PANC-1 xenografts (n ≥ 15), for indicated time points, with NADK knockdown and rescue with either WT NADK or mutant NADK.

(E) Relative NADP(H) levels in PDEs expressing the indicated NADK phosphomutants and treated with PMA, as previously described in (A). n ≥ 4.

(F) Labeling of NADP+ and NADPH from [^{2}H]NAM in PDEs expressing S46A/S64A mutant. Cells treated as previously described in (A). n = 4.

(G) Relative NADP(H) levels in PDEs expressing the indicated NADK phosphomutants, but in this case, single phosphomutants, and treated with PMA, as previously described in (A). n ≥ 4.

(H) Graph of *in vitro* NADK activity assay for single S46A and S64A mutants purified from HEK293A cells treated with PMA as previously described in (A). n = 3.

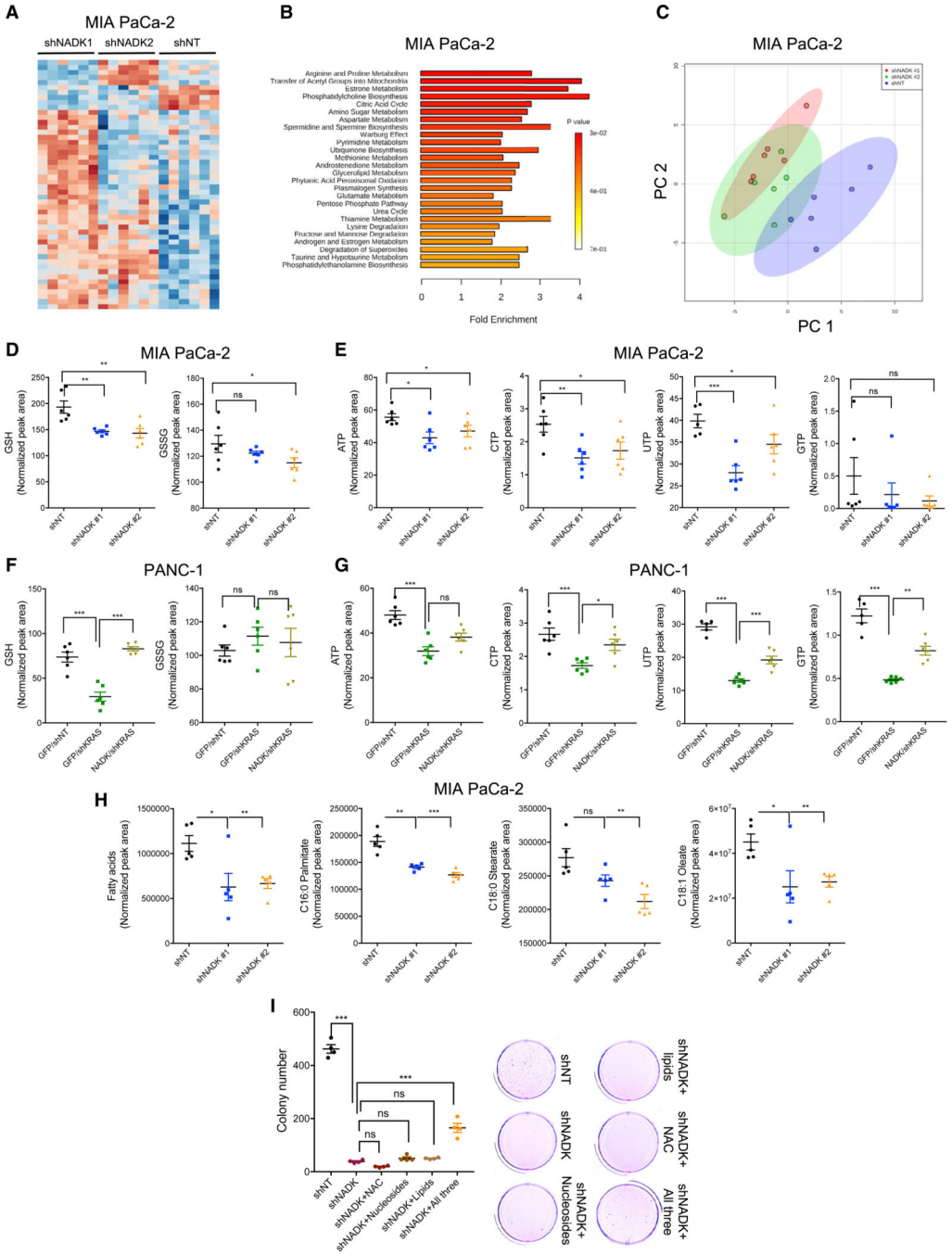

Figure 4. NADK sustains cell growth and drives stress resistance to promote PDAC

(A) Heatmap of metabolites extracted from MIA PaCa-2-expressing shNT (non-targeting) and shNADK #1 and #2.

(B) Pathway analysis of MIA PaCa-2 metabolites upon NADK knockdown.

(C) Principal-component analysis of MIA PaCa-2 metabolites upon NADK knockdown.

(D) Relative oxidized and reduced glutathione levels in MIA PaCa-2 upon NADK knockdown. n ≥5.

(E) Relative nucleotide levels as in (D). n ≥5.

(F) Relative oxidized and reduced glutathione levels in PANC-1 upon KRAS knockdown ± NADK overexpression. n ≥ 5.

(G) Relative nucleotide levels as in (F). n ≥5.

(H) Relative levels of global and distinct species of fatty acids upon knockdown of NADK in MIA PaCa-2. n = 5.

(I) Colony-forming capacity in MIA PaCa-2 expressing shNADK and treated with 2 mM N-acetyl-L-cysteine (NAC), 5 mg/L nucleosides, or 12 μg/ml LDL and 50 μM oleate, each alone or in combination for the duration of the assay. n = 4.

KEY RESOURCES TABLE

REAGENT or RESOURCE	SOURCE	IDENTIFIER
Antibodies		
NADK	Cell Signaling	55948S; RRID:AB_2799500
NADK	Bethyl Laboratories	A304−993A; RRID:AB_2621187
PKC Substrate	Cell Signaling	6967S; RRID:AB_10949977
PKA Substrate	Cell Signaling	9624S; RRID:AB_331817
AKT Substrate	Cell Signaling	10001S; RRID:AB_10950819
RASG12D	Cell Signaling	14429S; RRID:AB_2728748
RASG12V	Cell Signaling	14412S; RRID:AB_2714031
RAS	Cell Signaling	3339S; RRID:AB_2269641
RAS	Cell Signaling	3965S; RRID:AB_2180216
FLAG	Thermo Fisher	MA1−91878-1MG; RRID:AB_2537619
PKC alpha	Cell Signaling	2056S; RRID:AB_2284227
PKC delta	Cell Signaling	2058S; RRID:AB_10694655
PKC beta	Santa Cruz	sc-209; RRID:AB_2168968
PKC gamma	Santa Cruz	sc-211; RRID:AB_632234
PKC theta	Santa Cruz	sc-212; RRID:AB_675807
PKC eta	Santa Cruz	sc-215; RRID:AB_2171769
PKC epsilon	Santa Cruz	sc-214; RRID:AB_2237729
Pan-PKC	Santa Cruz	sc-17769; RRID:AB_628139
HA	Santa Cruz	sc-7392; RRID:AB_627809
pMARCKS S159/153	Cell Signaling	11992S; RRID:AB_2797791
pMARCKS S152/156	Cell Signaling	2741S; RRID:AB_2140318
pMARCKS S167/170	Cell Signaling	8722S; RRID:AB_10999091
MARCKS	Cell Signaling	5607S; RRID:AB_10547885
Vinculin	Sigma-Aldrich	V9264; RRID:AB_10603627
pERK1/2 T202/Y204	Cell Signaling	4370L; RRID:AB_2315112
ERK1/2	Cell Signaling	4696S; RRID:AB_390780
pAKT T308	Cell Signaling	13038S; RRID:AB_2629447
pAKT S473	Cell Signaling	4060L; RRID:AB_2315049

Cell Rep. Author manuscript; available in PMC 2025 May 14.

REAGENT or RESOURCE	SOURCE	IDENTIFIER
AKT	Cell Signaling	4691S; RRID:AB_915783
EGFR	Cell Signaling	2239S; RRID:AB_331373
COXIV	Cell Signaling	4850S; RRID:AB_2085424
GAPDH	Sigma-Aldrich	G8795−200UL; RRID:AB_1078991
pNADK S64	Abcam	N/A
anti-Rabit HRP secondary	GE Healthcare	NA934; RRID:AB_772206
anti-Mouse HRP secondary	GE Healthcare	NA931; RRID:AB_772210
anti-Goat HRP secondary	Millipore	AP180P; RRID:AB_92573
Monoclonal anti-HA-agarose antibody	Sigma-Aldrich	A2095−1ML; RRID:AB_257974
Bacterial and virus strains		
Adenoviral Cre	SignaGen Laboratories	SL100707
Chemicals, peptides, and recombinant proteins		
Recombinant Human EGF	Peprotech	AF-100−15
Penicillin-Streptomycin	Thermo Fisher	15140−163
Trypsin	Life Technologies	25300120
tert-Butyl hydroperoxide	Sigma-Aldrich	458139−25ML
N-acetyl-L-cysteine (NAC)	Sigma-Aldrich	A9165−5G
phorbol 12-myristate 13-acetate (PMA)	Cayman Chemical Company	10008014
Human insulin solution	Sigma-Aldrich	I9278−5ML
Sotrastaurin (SOT)	SelleckChem	S2791
Ionomycin	Sigma-Aldrich	I9657−1MG
HYDROGEN PEROXIDE 30% (W/W) SOLUTION (H_2O_2)	Sigma-Aldrich	H1009−100ML
KN-93 Phosphate (KN-93)	SelleckChem	S7423
PF4708671	Sigma-Aldrich	PZ0143
BID1870	Enzo Life Sciences	BML-EI407−0005
Selumetinib (AZD6244)	SelleckChem	S1008
MK2206	SelleckChem	S1078
CHIR 99021	SelleckChem	S2924
GDC0941	SelleckChem	S1065

REAGENT or RESOURCE	SOURCE	IDENTIFIER
Torin 1	Tocris	4247
HA peptide	Sigma-Aldrich	I2149−1MG
Sodium pyruvate	Life Technologies	11360−070
L-Glutamine solution	Sigma-Aldrich	G7513−100ML
Penicillin-Streptomycin	Thermo Fisher	15140−163
Gastrin I	Sigma-Aldrich	G9145-.1MG
Murine EGF	Peprotech	315−09-100ug
Murine R-Spondin-1	Peprotech	315−32
Murine Noggin	Peprotech	250−38-100ug
human FGF-10	Peprotech	100−26-50ug
Nicotinamide	Sigma-Aldrich	N0636−100G
TrypLE Express Enzyme	Thermo Fisher	12604−013
Y27632	Sigma-Aldrich	Y0503−1MG
Adenosine 5′-triphosphate magnesium salt (ATP)	Sigma-Aldrich	A9187−1G
Glucose 6-phosphate	Sigma-Aldrich	G7879−5G
Beta-Nicotinamide adenine dinucleotide (NAD+)	Sigma-Aldrich	N0632−5G
Human glucose 6-phosphate dehydrogenase (G6PD)	Sigma-Aldrich	SRP6505−100UG
ATP stock solution	SignalChem	A50−09-200
PKC Lipid Activator, 10x	SignalChem	L51−39-500
PKC gamma, Active	SignalChem	P66−10G-05
PKC delta, Active	SignalChem	P64−10G-10
PKC alpha, Active	SignalChem	P61−18G-05
Polybrene	Sigma-Aldrich	H9268
[2,4,5,6-^{2}H]nicotinamide ([^{2}H]NAM)	Cambridge Isotope Laboratories	DLM-6883−0.5
Formic Acid	Sigma-Aldrich	5330020050
Hexane	VWR	EM-HX0290P-1
Doxycycline	Millipore	324385
G418 Disulfate	Caisson Labs	G030
Hygromycin B	Thermo Fisher	10687−010
Blasticidin S HCl	Thermo Fisher	A11139−03
Puromycin	Sigma-Aldrich	P7255

REAGENT or RESOURCE	SOURCE	IDENTIFIER
Critical commercial assays		
QuikChange II XL site directed mutagenesis kit	Agilent Technologies	200521
LR Clonase II Enzyme Mix	Life Technologies	11791−100
BP Clonase II Enzyme Mix	Life Technologies	11789−100
X-tremeGENE HP	Roche	06366546001
Lipofectamine RNAiMAX Transfection Reagent	Life Technologies	13778150
SuperSep Phos-tag (50 μmol/L), 7.5%	VWR	103012−118
Subcellular Protein Fractionation Kit for Cultured Cells	Thermo Fisher	78840
CM-H2DCFDA	Thermo Fisher	C6827
Amicon Ultra-4 Centrifugal Filter Units	Millipore	UFC801024
SimplyBlue SafeStain	Thermo Fisher	LC6060
NADP/NADPH-Glo Assay	Promega	G9082
Experimental models: Cell lines		
hTERT-HPNE E6/E7/st (PDE)	ATCC	CRL-4037
MIA PaCa-2	ATCC	CRL-1420
PANC-1	ATCC	CRL-1469
BxPC3	ATCC	CRL-1687
A549	ATCC	CCL-185
A-375	ATCC	CRL-1619
SK-MEL-28	Gift from Dr. Lewis Cantley	N/A
NCI-H1975	Gift from Dr. Lewis Cantley	N/A
HEK293T	GenHunter	Q401
HEK293A	Thermo Fisher	R705−07
KP MEFs	Gift from Dr. Gina DeNicola	N/A
Experimental models: Organisms/strains		
$Kras^{+/LSL\text{-}G12D}$ C57BL/6	Gift from Dr. Lukas Dow	N/A
Female and male nu/nu athymic mice (Hsd:Athymic Nude-*Foxn1*^{nu})	Envigo	069
Oligonucleotides		
Primer to clone HA tag onto NADK N terminus Fw: TAAGCAGTCGACATGTACCCATACGATGTTCCAGATT	This paper	N/A

REAGENT or RESOURCE	SOURCE	IDENTIFIER
ACGCTATGGAAATGGAACAAGAAAAAATGACCATGAATAA		
Primer to clone HA tag onto NADK N terminus Rv: TGCTTACTCGAGTCATTACTAGCCCTCCTCCTCCTCCTC	This paper	N/A
Recombinant DNA		
pWZL-Neo-Myr-Flag NADK	Addgene	20415
pENTR1A	Addgene	17398
pLenti CMV Hygro DEST	Addgene	17454
pLenti PGK Hygro DEST	Addgene	19066
pLenti HA NADK WT or mutants	This paper	N/A
pENTRY-GFP	Addgene	15301
pDONR223 KRAS^{G12V}	Addgene	31200
pInducer20	Addgene	44012
pInducer20 GFP	This paper	N/A
pInducer20 KRAS^{G12V}	This paper	N/A
pLKO.1-puro shGFP	Sigma-Aldrich	TRCN0000072181
pLKO.1-puro Non-Mammalian shRNA Control	Sigma-Aldrich	SHC002
pLKO.1-blast	Addgene	26655
shNADK#1	Sigma-Aldrich	TRCN0000037700
shNADK#2	Sigma-Aldrich	TRCN0000199808
shNADK#3	Sigma-Aldrich	TRCN0000199040
shNadk#1	Sigma-Aldrich	TRCN0000297518
shNadk#2	Sigma-Aldrich	TRCN0000278616
shKRAS#1	Sigma-Aldrich	TRCN0000369099
shKRAS#2	Sigma-Aldrich	TRCN0000033260
psPAX2	Addgene	12260
pMD2.G	Addgene	12259
Software and algorithms		
SEQUEST (version 28, revision 13)	Eng et al., 1994	N/A
Prism 8	GraphPad	N/A
MultiQuant v2.0	AB/SCIEX	N/A

REAGENT or RESOURCE	SOURCE	IDENTIFIER
MetaboAnalyst	https://www.metaboanalyst.ca/	
Skyline (version 4.2.0.19072)	MacLean et al., 2010	N/A
MAVEN	http://genomics-pubs.princeton.edu/mzroll/index.php	N/A
AccuCor	Su et al., 2017	N/A
Other		
INCELL M3:Base F	INCELL	NC9920596
DMEM, high glucose	Life Technologies	11965118
DMEM, low glucose, pyruvate, HEPES	Life Technologies	12320−032
2x DMEM	Millipore	SLM-202-B
Advanced DMEM/F-12	Thermo Fisher	12634010
Corning Growth factor reduced Matrigel (GFR Matrigel)	VWR	47743−720
B27 supplement	Thermo-Fisher	17504044
Cell Recovery Solution	Corning	354253
Fetal bovine serum	Sigma-Aldrich	12303C
Dialyzed fetal bovine serum	Sigma-Aldrich	F0392−500ML
SeaPlaque Agarose	VWR	12001−900
EmbryoMax Nucleosides	EMD Millipore	ES-008-D
Low density lipoprotein	Sigma-Aldrich	L7914−5MG
Oleate	Sigma-Aldrich	O7501−250MG
SIC001 Mission siRNA Universal Negative Control	Sigma-Aldrich	SIC001−10NMOL
esiRNA PKC alpha	Sigma-Aldrich	EHU050821
esiRNA PKC beta	Sigma-Aldrich	EHU069171
esiRNA PKC gamma	Sigma-Aldrich	EHU034121
esiRNA PKC delta	Sigma-Aldrich	EHU067061